Anticrossing Spin Dynamics of Diamond Nitrogen-Vacancy Centers and All-Optical Low-Frequency Magnetometry

David A. Broadway,[1] James D. A. Wood,[1] Liam T. Hall,[2] Alastair Stacey,[1,3] Matthew Markham,[3] David A. Simpson,[2] Jean-Philippe Tetienne,[1,*] and Lloyd C. L. Hollenberg[1,2]

[1]*Centre for Quantum Computation and Communication Technology, School of Physics, The University of Melbourne, Melbourne, Victoria 3010, Australia*

[2]*School of Physics, The University of Melbourne, Melbourne, Victoria 3010, Australia*

[3]*Element Six Innovation, Fermi Avenue, Harwell Oxford, Didcot, Oxfordshire OX110QR, United Kingdom*

(Received 14 July 2016; revised manuscript received 25 September 2016; published 2 December 2016)

We investigate the photoinduced spin dynamics of single nitrogen-vacancy (N-V) centers in diamond near the electronic ground-state level anticrossing (GSLAC), which occurs at an axial magnetic field around 1024 G. Using optically detected magnetic resonance spectroscopy, we first find that the electron-spin transition frequency can be tuned down to 100 kHz for the ^{14}N-V center, while, for the ^{15}N-V center, the transition strength vanishes for frequencies below about 2 MHz owing to the GSLAC structure. Using optical pulses to prepare and read out the spin state, we observe coherent spin oscillations at 1024 G for the ^{14}N-V center which originate from spin mixing induced by residual transverse magnetic fields. This effect is responsible for limiting the smallest observable transition frequency, which can span 2 orders of magnitude ranging from 100 kHz to tens of megahertz, depending on the local magnetic noise. A similar feature is observed for the ^{15}N-V center at 1024 G. As an application of these findings, we demonstrate all-optical detection and spectroscopy of externally generated fluctuating magnetic fields at frequencies ranging from 8 MHz down to 500 kHz using a ^{14}N-V center. Since the Larmor frequency of most nuclear-spin species lies within this frequency range near the GSLAC, these results pave the way towards all-optical, nanoscale nuclear magnetic resonance spectroscopy, using longitudinal spin cross-relaxation.

DOI: 10.1103/PhysRevApplied.6.064001

I. INTRODUCTION

Detection and identification of spin species using established techniques such as magnetic resonance spectroscopy proves to have a host of applications in materials science, chemistry, and biology. However, these techniques are limited in sensitivity and thus require macroscopic ensembles of spins in order to produce a measurable signal [1]. A variety of techniques have been developed over the last decade to extend magnetic resonance spectroscopy to the nanometer scale [2–6]. Notably, methods based on the nitrogen-vacancy (N-V) center in diamond [7] have attracted enormous interest owing to their ability to operate under conditions compatible with biological samples [6,8]. While significant progress has been made with N-V–based sensing in the last few years [5], spectroscopy at the single nuclear spin level remains a major challenge [9–11].

The detection of external spins with the N-V center is generally achieved through measuring the longitudinal-spin-relaxation rate (T_1 processes) [12–16] or the transverse-spin-relaxation rate (dephasing, or T_2 processes) [15,17–19] of the N-V center's electron spin, as they are sensitive to the magnetic field fluctuations produced by the target spins [20–22]. To obtain spectral information on the target spins, most studies to date have focused on using T_2-based techniques, which have been applied to the spectroscopy of small ensembles of either electronic [23–26] or nuclear spins [9,11,27–29]. However, spectroscopic information can also be obtained from T_1 processes, via cross-relaxation between a probe spin (the N-V center's electron spin) and the target spins [30–36]. The T_1-based approach to quantitative spectroscopy introduced in Ref. [35] allows for nanoscale, all-optical, wideband magnetic resonance spectroscopy [36]. As such, it represents a promising alternative to T_2-based approaches, as the latter require radio-frequency (rf) driving of the probe and/or the target, which poses various technical challenges in addition to limiting the accessible frequency range.

In cross-relaxation spectroscopy, the T_1 of the N-V spin is monitored while we vary the strength of an applied axial magnetic field, B_z [Fig. 1(a)]. When the transitional energy between two of the N-V eigenstates (generally $|0_e\rangle$ and $|-1_e\rangle$, where the number refers to the electron spin projection m_e) is equal to that of a target spin [Fig. 1(b)], cross-relaxation occurs, which results in an increase in the relaxation rate, $1/T_1$, of the N-V center [35,36]. This increase can be measured by purely optical means, even for a single N-V center [13–16]. By scanning across a range of magnetic field strengths, a resonance spectrum of the target spins can be obtained, which can be deconvolved to

*jtetienne@unimelb.edu.au

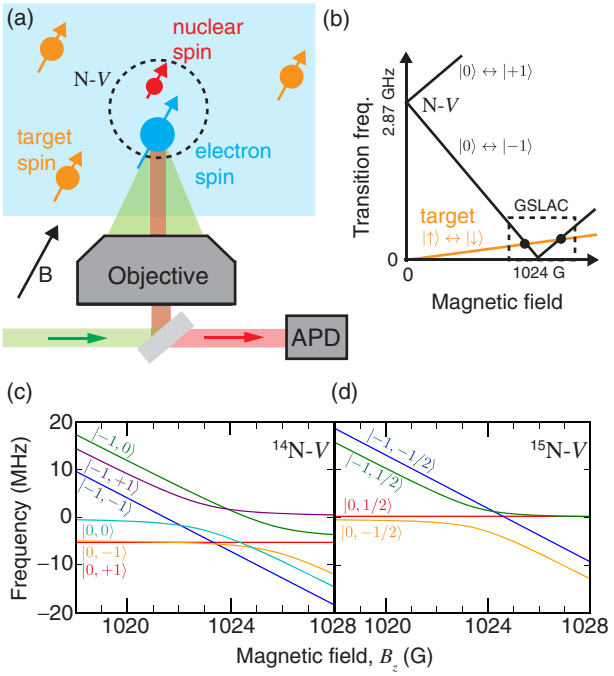

FIG. 1. (a) Schematic view of the system under study. The N-V center in diamond comprises a nuclear spin and an electron spin, which can be initialized and read out optically using a confocal microscope equipped with an avalanche photodiode (APD); it is surrounded by target spins located within the diamond or external to it. A magnetic field of strength B_z is applied along the N-V–quantization axis. (b) Schematic diagram showing the transition frequencies of the N-V electron spin (the black lines) and of a target nuclear spin (the orange line) as B_z is varied, with the resonance points shown as dots. The spin states are labeled by their spin projection, $|m_e = 0, \pm 1\rangle$ for the N-V electron, $|m_t = \uparrow, \downarrow\rangle$ for the target spin. (c),(d) Calculated hyperfine structure for the (c) ^{14}N-V and (d) ^{15}N-V centers, plotted near the GSLAC where the two branches $m_e = 0$ and $m_e = -1$ cross. The different states are labeled as $|m_e, m_n\rangle$, where m_e (m_n) is the electronic- (nuclear-) spin projection of the unperturbed states (away from the GSLAC). Owing to hyperfine interaction, some of the energy levels exhibit an avoided crossing at the GSLAC.

produce the target spin spectrum [35]. This technique was recently used to measure electronic-spin-resonance spectra of P1 centers within the diamond at magnetic fields of 460–560 G, corresponding to transition frequencies of 1300–1600 MHz [35,36]. In order to detect nuclear magnetic resonances (NMRs), the N-V transition frequency must be matched to the Larmor frequency of the target nuclear spins [Fig. 1(b)], which is generally on the order of a few megahertz. This matching occurs when the states $|0_e\rangle$ and $|-1_e\rangle$ approach degeneracy, at a magnetic field $B_z \approx 1024$ G. However, in this region, the N-V center experiences a complex ground-state level anticrossing (GSLAC) [Figs. 1(c) and 1(d)] [37] due to a hyperfine interaction of the N-V electron spin with its own nuclear spin (spin-1 ^{14}N or spin-$\frac{1}{2}$ ^{15}N; stable spin-free isotopes of nitrogen do not exist), which also has a coupling strength of several megahertz. The hyperfine interaction causes spin mixing, which may prevent the N-V electron spin from being initialized and readout [38]. Therefore, a detailed understanding of the spin dynamics at the GSLAC is required to assess the potential for performing T_1-based spectroscopy of nuclear spins, as was initially explored in Ref. [36]. While the GSLAC of the N-V center was previously studied and exploited in various works [37–44], there is little knowledge about how T_1 varies and how the spin dynamics (including optical initialization) behaves at transition frequencies relevant to T_1 NMR, close to the GSLAC.

In this paper, we investigate the spin dynamics at the GSLAC for both ^{14}N-V and ^{15}N-V spin systems in various diamond samples. We begin by looking at the computed energy spectra of both spin systems and compare them to optically detected magnetic resonance (ODMR) measurements at their respective GSLACs. The short-time spin dynamics of the ^{14}N-V spin at the GSLAC are probed using optical pulses, revealing a feature at $B_z \approx 1024$ G which manifests itself in either coherent spin oscillations or in a simple polarization drop, depending on the sample. This feature is explained by spin mixing induced by residual transverse magnetic fields. The ^{15}N-V center shows a similar feature at $B_z \approx 1024$ G. Apart from these narrow features, we find that the spin polarization and the T_1 time remain essentially constant across the GSLAC, implying that the N-V center can be used to detect magnetic signals at low frequencies via T_1 measurements. Finally, we demonstrate one such application by performing all-optical spectroscopy of fluctuating magnetic fields generated at known frequencies, mimicking those of nuclear spins. This demonstration suggests that it is possible to perform NMR spectroscopy via longitudinal cross-relaxation near the GSLAC.

II. ENERGY LEVELS OF THE N-V CENTER AT THE GSLAC

The N-V spin system consists of a nitrogen atom adjacent to a vacancy in the carbon lattice of diamond. It comprises a pair of electrons (forming a spin-1 particle) and a nuclear spin, which is a spin-1 particle for ^{14}N-V and a spin-$\frac{1}{2}$ particle for ^{15}N-V [Fig. 1(a)]. Owing to spin-spin interaction, the electronic spin states $|\pm 1_e\rangle$ are split from $|0_e\rangle$ by $D/2\pi \approx 2.87$ GHz. The degeneracy of the $|\pm 1_e\rangle$ doublet can be lifted by the application of an external magnetic field along the N-V center's symmetry axis, defined as the z axis [Fig. 1(b)]. The $|-1_e\rangle$ and $|0_e\rangle$ states cross at a field around $B_z = D/\gamma_e \approx 1024$ G (where γ_e is the electron gyromagnetic ratio). However, hyperfine interaction with the nitrogen nuclear spin causes an avoided crossing, the GSLAC [the dashed box in Fig. 1(b)], which is the main focus of this paper.

The energy spectrum of the N-V electronic ground state near the GSLAC can be found by solving for the eigenvalues of the spin Hamiltonian. The relevant Hamiltonians for the ^{14}N-V and ^{15}N-V cases, expressed in units of angular frequencies, are

$$\mathcal{H}(^{14}\text{N-}V) = DS_z^2 + \gamma_e B_z S_z - \gamma_n B_z I_z + QI_z^2 + A_\parallel S_z I_z + A_\perp (S_x I_x + S_y I_y), \quad (1)$$

$$\mathcal{H}(^{15}\text{N-}V) = DS_z^2 + \gamma_e B_z S_z - \gamma'_n B_z I'_z + A'_\parallel S_z I'_z + A'_\perp (S_x I'_x + S_y I'_y), \quad (2)$$

where $\mathbf{S} = (S_x, S_y, S_z)$ is the electron spin operator, $\mathbf{I}$ is the nuclear spin operator, and γ_n is the nuclear gyromagnetic ratio. The magnetic field is aligned along the N-V axis, with strength B_z. The primed symbols refer to the ^{15}N-V case. The longitudinal and transverse hyperfine parameters are denoted as $A_\parallel$ and $A_\perp$, whose values are $A_\parallel/2\pi = -2.14$ MHz and $A_\perp/2\pi = -2.7$ MHz for the ^{14}N-V center, and $A'_\parallel/2\pi = 3.03$ MHz and $A'_\perp/2\pi = 3.65$ MHz for the ^{15}N-V center [45]. In addition, the ^{14}N-V center has a quadrupole coupling with the strength $Q/2\pi = -5.01$ MHz [45].

The energy spectrum is obtained by evaluating the eigenvalues of the Hamiltonian at different axial field strengths B_z and is shown in Fig. 1(c) for the ^{14}N-V center and Fig. 1(d) for the ^{15}N-V center. The manifold associated with the spin projection $|+1_e\rangle$ is not shown, as it lies about 6 GHz above the manifold spanned by $|0_e\rangle$ and $|-1_e\rangle$ and does not contribute to the effects discussed in this paper. We thus consider only the six lower-energy states for the ^{14}N-V center, and the four lower states for the ^{15}N-V center. Away from the GSLAC, the eigenstates have well-defined spin projections along the z axis. In the electron- and nuclear-spin space, we denote states as $|m_e, m_n\rangle$, where m_e (m_n) is the electronic- (nuclear-) spin projection along the z axis. The hyperfine coupling between the N-V nuclear and electron spins results in a splitting of the nuclear-spin states for each electronic spin state due to the longitudinal component $A_\parallel$. Near the GSLAC, the perpendicular component of the hyperfine ($A_\perp$) induces a mixing of some of the z-basis states. This effect is noticeable when the quantization energy between said states becomes of the order $A_\perp$. In the case of the ^{14}N-V center, the states $|0,+1\rangle$ and $|-1,-1\rangle$ do not mix, as they have no hyperfine coupling to any other state (due to their respective total spin projection being unique in this energy range [46]) and, as such, they remain eigenstates. The rest of the N-V states are mixed: that is, the eigenstates are superpositions of z-basis states, creating an avoided crossing. The ^{15}N-V spin also exhibits mixing at the GSLAC. For example, the $|0,-1/2\rangle$ and $|-1,+1/2\rangle$ states become mixed, while the $|0,+1/2\rangle$ and $|-1,-1/2\rangle$ states remain eigenstates.

III. OPTICALLY DETECTED MAGNETIC RESONANCE AT THE GSLAC

Experimentally, one can probe the N-V energy spectrum using ODMR spectroscopy [47]. The spectrum is achieved by measuring the photoluminescence (PL) intensity of the N-V center while varying the frequency of an applied rf field, using a purpose-built confocal microscope with green-laser excitation [Fig. 1(a)]. The laser serves both to initialize the N-V in the electronic spin state $|0_e\rangle$ and to read out the spin state following a rf pulse, exploiting the fact that $|\pm 1_e\rangle$ spin states emit less PL, on average, than $|0_e\rangle$ states [48]. Thus, ODMR allows us to probe the electron spin transitions $|0_e\rangle \rightarrow |\pm 1_e\rangle$. We record ODMR spectra for magnetic fields that vary, from 1018 to 1032 G, for single ^{14}N-V and ^{15}N-V centers in a high-purity diamond grown by chemical vapor deposition (CVD). The magnetic field is aligned with the N-V quantization axis to $< 0.1°$ by relying on the angle-dependent PL intensity [38,49] (see the experimental setup and related details in Ref. [36]).

The results of the ODMR scans are shown in Fig. 2, where the top (bottom) panels show the $|0_e\rangle \rightarrow |+1_e\rangle$ ($|0_e\rangle \rightarrow |-1_e\rangle$) transitions. The left (right) panels correspond to a ^{14}N-V (^{15}N-V) center. Comparing our results

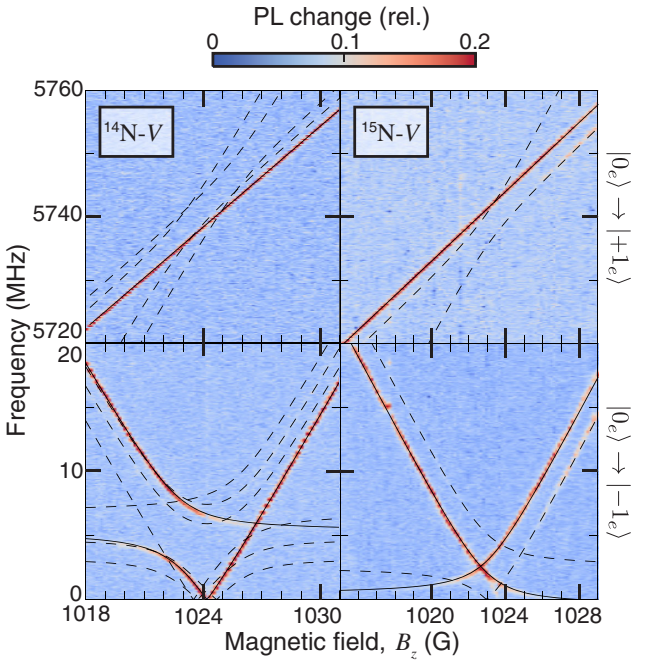

FIG. 2. ODMR spectra of (left panels) a ^{14}N-V and (right panels) a ^{15}N-V center, measured as a function of the axial-magnetic field strength near the GSLAC. The top panels show the electron spin transitions $|0_e\rangle \rightarrow |+1_e\rangle$, while the bottom panels show $|0_e\rangle \rightarrow |-1_e\rangle$. Overlaid on the graph are the theoretical frequencies of all allowed or partly allowed (via spin mixing) transitions. However, dynamic nuclear-spin polarization makes some of the transitions dominant (shown as solid lines), with the other transitions having comparatively small or vanishing contrast (the dashed lines).

with the theoretical expectations for the allowed transitions (shown as black lines), it can be seen that only a limited number of expected transitions are observed experimentally. This result occurs because the nuclear spin is efficiently polarized under optical pumping near the GSLAC, owing to hyperfine-induced spin mixing. This dynamic nuclear polarization effect has been well documented for ^{14}N-V and ^{15}N-V centers at the excited-state level anticrossing (ESLAC) [50,51], and the effect has been observed for a strongly coupled ^{13}C spin at the GSLAC [42]. It originates from polarization transfer from the N-V electron spin ($|-1_e\rangle \rightarrow |0_e\rangle$ due to optical pumping) to the nuclear spin ($|m_n\rangle \rightarrow |m_n+1\rangle$) under near-resonant conditions. Using the relative strengths of the $|0_e\rangle \rightarrow |+1_e\rangle$ ODMR transitions (the top panels in Fig. 2), we find that the nuclear spin is polarized to $> 90\%$ into $|+1_n\rangle$ for this ^{14}N-V center across the whole range of fields scanned here. For the ^{15}N-V center investigated in Fig. 2, the nuclear spin is polarized to $> 90\%$ in $|+1/2_n\rangle$ up to $B_z \approx 1026$ G, but it becomes completely unpolarized above $B_z \approx 1028$ G.

We now discuss the ODMR spectrum of the $|0_e\rangle \rightarrow |-1_e\rangle$ transitions (the bottom panels in Fig. 2). For the ^{14}N-V center, the spin is efficiently polarized in the state $|0,+1\rangle$, which remains an eigenstate at all fields. Away from the GSLAC, the only transition allowed is to the state with the same nuclear-spin projection, $|-1,+1\rangle$. However, near the GSLAC, the state $|-1,+1\rangle$ becomes mixed with $|0,0\rangle$, which creates two eigenstates of the forms $|+\rangle = \alpha|-1,+1\rangle + \beta|0,0\rangle$ and $|-\rangle = \beta|-1,+1\rangle - \alpha|0,0\rangle$, where $(|\alpha|^2, |\beta|^2)$ continuously changes from (1,0) to (0,1) upon passing the GSLAC [38,42]. This mixing results in an avoided crossing feature centered at $B_z \approx 1022$ G, around the transition frequency $\omega \approx 5$ MHz which corresponds to the quadrupole coupling Q. Conversely, there is little mixing at the allowed crossing at $B_z \approx 1024$ G, which means that the dominant transition here is $|0,+1\rangle \rightarrow |-1,+1\rangle$. We observe clear ODMR signatures with resonance frequencies down to 100 kHz in this sample. This observation implies that the N-V spin could be resonantly coupled to most nuclear-spin species, which have Larmor frequencies ranging typically from 500 kHz to 5 MHz at this magnetic field. However, the minimum observable transition frequency is found to be highly sample dependent, as is discussed in Sec. IV.

On the other hand, the ^{15}N-V center exhibits a very different spectrum near the GSLAC (Fig. 2, right-hand panels). Under optical pumping, it is efficiently polarized in the state $|0,+1/2\rangle$, which remains an eigenstate at all fields. The states it can transit to under rf driving are superpositions of the forms $|+\rangle = \alpha|-1,+1/2\rangle + \beta|0,-1/2\rangle$ and $|-\rangle = \beta|-1,+1/2\rangle - \alpha|0,-1/2\rangle$, where the avoided crossing is centered approximately around the initial state $|0,+1/2\rangle$ [see Fig. 1(d)]. As a result, the ODMR plot shows two transitions that bend upon approaching vanishing frequencies. They cross at a field $B_z \approx 1024$ G and a transition frequency $\omega'_\times/2\pi \approx 2.65(2)$ MHz, as determined from Fig. 2. This crossing frequency can be analytically derived from diagonalizing the Hamiltonian (2) and equating the two relevant spin transition frequencies [52], which yields

$$\omega'_\times = \sqrt{\frac{A'^2_\perp}{2} + \left(\frac{\gamma'_n}{\gamma_e - \gamma'_n}\right)^2 \left(D - \frac{A'_\parallel}{2}\right)^2}. \tag{3}$$

Incidentally, this equation allows the perpendicular component of the hyperfine interaction ($A'_\perp$) to be measured directly on a single ^{15}N-V center, which gives here $A'_\perp/2\pi = 3.69(3)$ MHz, in excellent agreement with the ensemble-averaged value of 3.65(3) MHz reported in Ref. [45]. The peculiar GSLAC structure of the ^{15}N-V center has important consequences for sensing. Specifically, the contrast of the transitions decreases rapidly for frequencies below $\omega'_\times$, as they become forbidden. As a result, the ^{15}N-V center is not suited for detecting resonances below about 2 MHz under typical conditions. Most nuclear-spin species have transitions within this range, with an exception being hydrogen (^{1}H), which has a Larmor frequency of about 4.4 MHz at this field and could, in principle, be detected via cross-relaxation with a ^{15}N-V center.

IV. PHOTOINDUCED SPIN DYNAMICS AT THE GSLAC

We now investigate the spin population dynamics near the GSLAC. Our aim is to assess the possibility of measuring the longitudinal-spin-relaxation time (T_1), as required in order to perform cross-relaxation spectroscopy and detect nearby nuclear spins [36]. The T_1 time is typically measured by using laser pulses to initialize the N-V center into $|0_e\rangle$, and to read out the remaining population of $|0_e\rangle$ after a variable delay t [Fig. 3(a)]. In practice, the PL signal is integrated at the start of the readout pulse (I_s) and normalized by the PL from the back of the pulse (I_r). The normalized signal I_s/I_r can be expressed as [48]

$$\frac{I_s}{I_r}(t) = a + bP_0(t), \tag{4}$$

where $P_0(t) = |\langle 0_e|\psi(t)\rangle|^2$ is the population in $|0_e\rangle$ of the current spin state $|\psi(t)\rangle$, and $a \approx 1$ and $b \approx 0.3$ are constants. The resulting time trace $(I_s/I_r)(t)$, therefore, allows us to estimate the initial population $P_0(0)$, which approaches unity under normal conditions [48], as well as the evolution of the spin state under free evolution (in the dark). In general (away from the GSLAC or the ESLAC), the spin population exhibits a simple exponential decay towards a thermal mixture; i.e., $P_0(t) = \frac{1}{3} + \frac{2}{3}e^{-t/T_1}$, assuming perfect initialization [see an example in

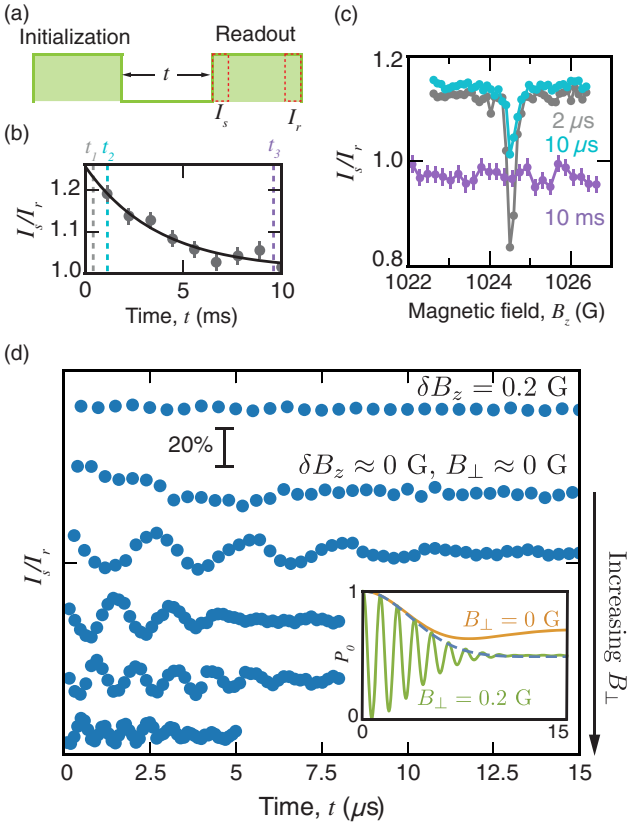

FIG. 3. (a) Depiction of the laser-pulse sequence used to measure the spontaneous spin dynamics, containing an initialization pulse and a readout pulse after a wait time t. (b) Time trace measured for a single ^{14}N-V center at a field $B_z = 1000$ G. Here, a decay with a characteristic time $T_1 \approx 5$ ms, associated with phonon relaxation, is observed. (c) Set of PL scans as a function B_z for various evolution times t, under a small residual transverse field $B_\perp$, showing a narrow feature at $B_z \approx 1024$ G. The evolution times $t = 2$ μs (gray), 10 μs (light blue), and 1 ms (purple) are indicated as dashed lines in (b), with exaggerated positions for ease of viewing. (d) Time traces recorded at $B_z \approx 1024$ G. The top curve is measured with a detuning $\delta B_z = 0.2$ G, showing no variation in the range $t = 0$–15 μs. The other curves are recorded with no detuning, but with a transverse magnetic field $B_\perp$ increasing from about 0 to approximately 0.5 G (top down). The curves are vertically offset from each other for clarity. (Inset) Averaged time traces $\langle P_0(t)\rangle$ computed from Eq. (6) where δB_z and $B_\perp$ are normally distributed, with mean values $\langle \delta B_z\rangle = 0$ and $\langle B_\perp\rangle = 0$ G (the orange curve) or 0.2 G (the green curve) and variances $\sigma_{B_z} = 1.3$ μT and $\sigma_{B_\perp} = \sqrt{3/4}\sigma_{B_z}$. The dashed blue line is the approximate envelope $e^{-(t/T_\times)^2}$, with $T_\times = (\gamma_e \sigma_{B_\perp})^{-1} = 5$ μs.

Fig. 3(b)]. In the following, we measure $(I_s/I_r)(t)$ for different evolution times t as a function of the axial magnetic field B_z.

A. ^{14}N-V centers

We first perform measurements of ^{14}N-V centers in an ultrahigh-purity CVD-grown diamond with isotopically purified carbon content ($[^{12}\mathrm{C}] > 99.99\%$). In this sample, the main source of magnetic noise comes from the bath of the remaining ^{13}C impurities [53]. A scan across the GSLAC for a representative ^{14}N-V center is shown in Fig. 3(c), where we probe three time points: $t = 2$ μs, 10 μs, and 10 ms. When the N-V is far from the GSLAC crossing, an exponential decay is observed, as shown in the full time trace in Fig. 3(b). This decay corresponds to phonon-induced relaxation, with a characteristic time $T_1 \approx 5$ ms [32]. At the crossing at $B_z \approx 1024$ G, however, a sharp variation in signal is observed [Fig. 3(c)]. Here, the N-V spin undergoes population oscillations, as indicated by the drop of the 2-μs time point below the 10-ms point.

To understand this oscillation, we express the Hamiltonian (1) in the basis that contains the states that cross, $\{|0,+1\rangle, |-1,+1\rangle\}$. In a magnetic field $\mathbf{B} = (B_x, B_y, B_z)$, the reduced Hamiltonian, $\mathcal{H}_R$, can be written as

$$\mathcal{H}_R = \begin{pmatrix} 0 & \gamma_e B_\perp \frac{e^{-i\theta}}{\sqrt{2}} \\ \gamma_e B_\perp \frac{e^{+i\theta}}{\sqrt{2}} & \gamma_e \delta B_z \end{pmatrix}, \tag{5}$$

where we introduce the axial detuning from the crossing, $\gamma_e \delta B_z = D - \gamma_e B_z - A_\parallel$, the transverse magnetic field, $B_\perp = \sqrt{B_x^2 + B_y^2}$, and the angle θ defined by $\tan\theta = B_y/B_x$. The transverse field causes a mixing between $|0,+1\rangle$ and $|-1,+1\rangle$ and opens an energy gap associated with a level avoided crossing. Assuming that optical pumping always initializes the N-V in the $|0,+1\rangle$ state —and reads out the population in that same state—we then expect oscillations between $|0,+1\rangle$ and $|-1,+1\rangle$ that are mirrored in the PL when in the presence of a transverse magnetic field. Under these conditions, the probability of occupying the state $|0,+1\rangle$ after an evolution time t following initialization is given by

$$P_0(t) = \frac{\delta B_z^2 + B_\perp^2[1 + \cos(\gamma_e t\sqrt{\delta B_z^2 + 2B_\perp^2})]}{\delta B_z^2 + 2B_\perp^2}. \tag{6}$$

The amplitude of the oscillation vanishes when the detuning is much larger than the transverse field ($\delta B_z \gg B_\perp$), far from the avoided crossing region. This regime is illustrated in Fig. 3(d) (the top curve), which is recorded with a detuning $\delta B_z \approx 0.2$ G $\gg B_\perp$. On the other hand, near the avoided crossing where the amplitude is maximal, the frequency of the oscillation is expected to increase as $B_\perp$ is increased. This effect is tested through a series of measurements with varying transverse fields. The experiment involves using a permanent magnet to align the field at the 1024-G crossing so that no oscillations are detected. The permanent magnet is then moved in the transverse direction (x or y) to add a transverse field. The results are shown in Fig. 3(d), where $B_\perp$ is increased from

the top down, resulting in faster oscillations. Although it is not possible to precisely calibrate the values of $B_\perp$, a rough estimate can be obtained by comparing the measured PL drop as a function of $B_\perp$ to the data from Ref. [38]. One finds that the largest $B_\perp$ applied in Fig. 3(d) (the bottom curve) corresponds to $B_\perp \sim 0.5$ G, and hence an oscillation frequency of approximately 2.8 MHz, according to Eq. (6). This result is in qualitative agreement with the measured frequency of approximately 1.6 MHz.

Damping of the oscillations is attributed to noise in the local magnetic field. In this sample, the noise comes predominantly from the bath of ^{13}C impurities. Examination of this interaction via the rotating-wave approximation shows that only the x-z, y-z, and z-z components of the dipole-dipole coupling to the N-V spin need be considered [54]. As such, the effective magnetic noise from the environment may be regarded as static over the short times, t, considered here. We assume that the field components δB_z and $B_\perp$ are normally distributed with mean values $\langle \delta B_z \rangle$ and $\langle B_\perp \rangle$ and variances $\sigma^2_{B_z}$ and $\sigma^2_{B_\perp}$, respectively. Averaging Eq. (6) over these distributions, we find numerically that the decay envelope of $\langle P_0(t) \rangle$ is well approximated by a Gaussian function $e^{-(t/T_\times)^2}$, where the characteristic time $T_\times$ is given by $T_\times^{-1} = \gamma_e \sigma_{B_\perp}$, regardless of the means $\langle \delta B_z \rangle$ and $\langle B_\perp \rangle$ [see the inset in Fig. 3(d)]. In other words, the damping of the 1024-G oscillations is mainly caused by the fluctuations in the transverse magnetic field. It is interesting to link this damping time $T_\times$ to the dephasing time T_2^* measured in a free-induction-decay (FID) experiment [54,55]. Under the same assumptions, the FID envelope takes the form $e^{-(t/T_2^*)^2}$, where $(T_2^*)^{-1} = \gamma_e \sigma_{B_z}/\sqrt{2}$. Moreover, a bath of randomly placed spins around the N-V center leads to $\sigma^2_{B_\perp} \approx \frac{3}{4}\sigma^2_{B_z}$, on average [54], which gives the relation

$$T_\times \approx T_2^* \sqrt{\frac{2}{3}}. \tag{7}$$

For the N-V center studied in Fig. 3, the damping time of the 1024-G oscillations is $T_\times \approx 5$–10 μs, estimated from the curves shown in Fig. 3(d); hence, $\sqrt{\frac{3}{2}} T_\times \approx 6$–$12$ μs. This time span is significantly shorter than the dephasing time $T_2^* > 50$ μs. We attribute the discrepancy mainly to drifts in the magnetic field applied during the measurements, which leads to our overestimating the damping rate $1/T_\times$.

We now consider the case where the magnetic field is aligned along the N-V axis, i.e., $\langle B_\perp \rangle = 0$. At the crossing when $\delta B_z = 0$, the averaged population $\langle P_0(t) \rangle$ does not oscillate, but still decays with a characteristic time $T_\times$ [see the inset in Fig. 3(d)]. However, the amplitude of the decay decreases as δB_z is increased. We define the width of the 1024-G feature, denoted $\Delta B_z^\times$, as twice the detuning δB_z to apply to obtain a maximum population drop of 20%. We find numerically that $\Delta B_z^\times \approx 4\sigma_{B_\perp}$, which can also be expressed as a function of T_2^* according to

$$\gamma_e \Delta B_z^\times \approx \frac{4}{T_\times} \approx \frac{2\sqrt{6}}{T_2^*}. \tag{8}$$

For the N-V center studied here, we predict a width $\Delta B_z^\times < 1$ μT for a perfectly aligned background field. We note, however, that, in the measurements of Fig. 3(c), the width is instead given by the residual transverse field [$B_\perp \approx 0.3$ G in Fig. 3(c)], which could not be maintained to significantly smaller values for extended periods of time due to drifts in the applied magnetic field.

The observation of coherent oscillations at the GSLAC suggests a direct application to dc magnetometry. Indeed, the frequency of the oscillation is directly proportional to the strength of the transverse field, according to Eq. (6), assuming that $\delta B_z \ll B_\perp$. For photon-shot-noise-limited measurements, the magnetic sensitivity is similar to that obtained by FID measurements [53], with the advantage of being an all-optical technique (as no microwave or rf field is required).

We now compare the spin dynamics of ^{14}N-V centers at the GSLAC in different diamond samples. Of particular relevance to sensing applications are N-V centers implanted close to the diamond surface. We perform measurements of shallow N-V centers in a CVD-grown diamond with natural isotopic concentration ($[^{13}\mathrm{C}] = 1.1\%$). The N-$V$ centers are created by implantation of N^+ ions with an energy of 3.5 keV, followed by annealing, resulting in N-V centers at a mean depth of 10 nm [56]. Figure 4(a) shows a scan across the GSLAC for a particular ^{14}N-V center. A reduction in the PL is observed at a field $B_z \approx 1024$ G, corresponding to the crossing discussed before. However, full time traces [shown in Fig. 4(b)] now reveal a simple offset of the PL at the crossing, with no obvious oscillatory behavior. This behavior can be understood by the large magnetic noise originating from the surface, which results in a decay time $T_\times$ shorter than the minimum probe time of $t = 1$ μs (limited by the lifetime of the singlet state [48]). The width of the feature in Fig. 4(a) is approximately 1 G (or approximately 3 MHz). By measuring various shallow N-V centers in the same sample, we find a range of widths of the 1024-G feature of 1 to 3 G (or 3 to 9 MHz). This variability is attributed to different local environments, especially because each N-V center sits at a different distance from the surface. For applications to the T_1-based NMR spectroscopy proposed in Ref. [36], this result implies that nuclear-spin species with large gyromagnetic ratios such as ^{1}H (Larmor frequency of approximately 4.4 MHz at 1024 G) can be resonantly coupled to a shallow ^{14}N-V center such as that measured in Fig. 4(a). However, species with smaller gyromagnetic ratios such as ^{13}C (a Larmor frequency of approximately 1.1 MHz) are generally

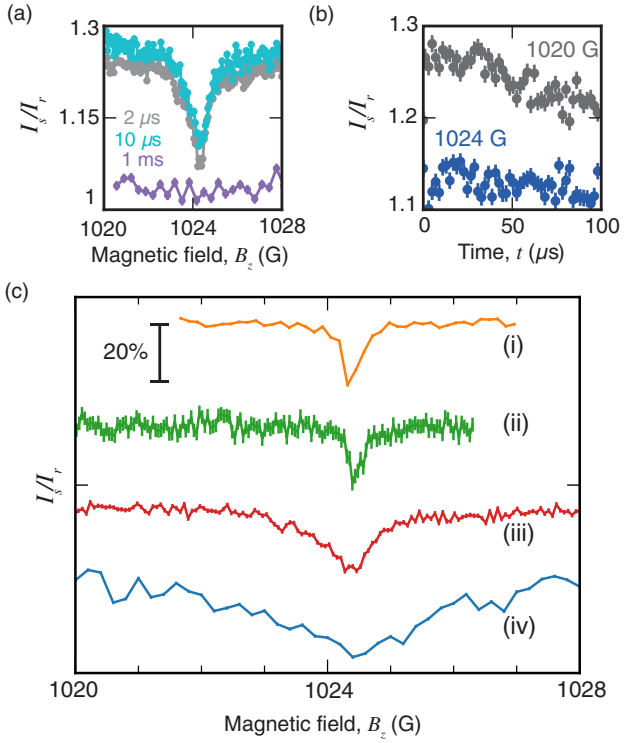

FIG. 4. (a) PL scan across the GSLAC for a shallow ^{14}N-V center in a CVD diamond, with evolution times $t = 2$ μs, 10 μs, and 1 ms. Here, no oscillation is detected, but an overall decrease in spin population is observed at $B_z \approx 1024$ G. (b) Time traces recorded at the crossing feature ($B_z \approx 1024$ G, the blue dots) and away from it ($B_z \approx 1020$ G, the gray dots). (c) PL scans across the GSLAC recorded with ^{14}N-V centers in various diamond samples. (i) Deep N-V center in isotopically purified CVD diamond, as in Fig. 3. (ii) Deep N-V center in natural-isotopic-content CVD diamond. (iii) Shallow N-V center in CVD diamond as in (a) and (b). (iv) Deep N-V center in type-Ib diamond. The curves are vertically offset from each other for clarity.

within the width of the crossing feature in the present sample, and could therefore hardly be detected via cross-relaxation. This realization motivates further progress in optimizing the coherence properties of shallow N-V spins, or devising ways to mitigate the effect of dephasing in T_1 measurements.

Finally, we measure the properties of ^{14}N-V centers at the GSLAC in two other settings: (1) deep ^{14}N-V centers in a CVD diamond with $[^{13}\mathrm{C}] = 1.1\%$, where decoherence is dominated by the ^{13}C bath rather than by surface effects, and (ii) deep ^{14}N-V centers in type-Ib diamond grown by the high-pressure high-temperature method, where the main source of decoherence is the bath of electronic spins associated with nitrogen impurities [57]. Sample scans across the GSLAC are shown in Fig. 4(c). Deep N-V centers in CVD diamond show linewidths of the 1024-G feature smaller than approximately 0.3 G for most N-V centers (approximately 1 MHz). By contrast, linewidths in the type-Ib diamond are of the order of 10–20 MHz, which makes such diamonds unsuited to T_1-based NMR spectroscopy.

B. ^{15}N-V centers

As previously discussed, the energy structure of the ^{15}N-V center at the GSLAC precludes it from accessing transition frequencies below about 2 MHz. Although this restriction limits the range of nuclear-spin species that could be resonantly coupled to the ^{15}N-V center, the highly relevant ^{1}H remains accessible. It is, therefore, important to test the ability to measure the T_1 of ^{15}N-V centers near the GSLAC.

As in the ^{14}N-V case, we record PL scans across the GSLAC with different evolution times, t. For this study, the measurements are performed on shallow ^{15}N-V centers in a CVD diamond only, as this sample is the most relevant one for sensing applications. The implantation energy is 3.5 keV and the concentration of ^{13}C is 1.1%, similar to the diamond used in Fig. 4(a). Figure 5(a) shows a scan obtained for a particular ^{15}N-V center. The spin population remains essentially constant across the GSLAC, except at a magnetic field $B_z \approx 1024$ G, where a sharp change is observed. Time traces at and away from the feature are shown in Figs. 5(b) and 5(c). While the long time scale reveals an exponential decay with a characteristic time $T_1 \approx 2$ ms independent from the magnetic field [Fig. 5(b)],

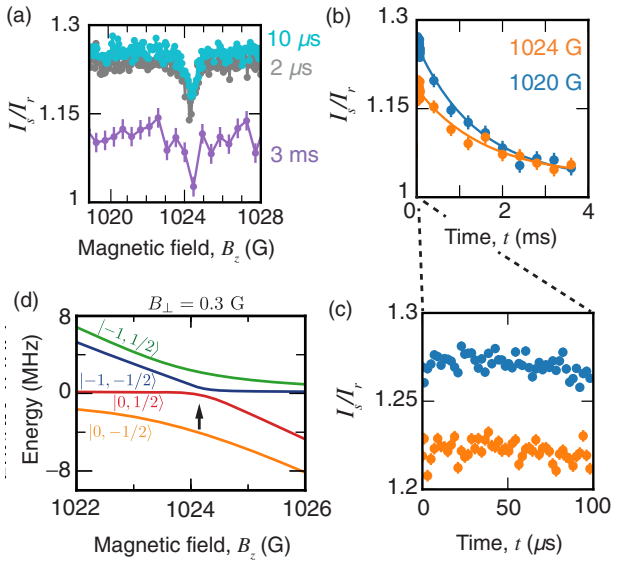

FIG. 5. (a) PL scan across the GSLAC for a shallow ^{15}N-V center in a CVD diamond, with evolution times $t = 2$ μs, 10 μs, and 3 ms. A feature at $B_z \approx 1024$ G is observed, attributed to spin mixing induced by transverse magnetic fields. (b),(c) Time traces recorded at the crossing feature ($B_z \approx 1024$ G, the orange dots) and away from it ($B_z \approx 1020$ G, the blue dots). The long and short time scales are shown in (b) and (c), respectively. (d) Energy-level structure of the ^{15}N-V center in the presence of a transverse magnetic field $B_\perp = 0.3$ G, showing an induced avoided crossing (indicated by the arrow).

the contrast of the decay is significantly smaller at $B_z \approx 1024$ G. This result is due to the initial population being lower, as can be seen from the drop of signal at short time scales [Fig. 5(c)]. This 1024-G feature is consistently seen in most of the ^{15}N-V centers investigated, exhibiting a variety of amplitudes and widths. At this field, the dominant N-V transition has a frequency of approximately 4.3 MHz. This feature is 1 G beyond the 1023-G crossing observed in the ODMR (see Fig. 2), when the N-V transition frequency is $\omega_\times' \approx 2.65$ MHz.

To understand this 1024-G feature, we consider the energy-level structure shown in Fig. 1(d). As mentioned previously, under optical pumping near the GSLAC, the ^{15}N-V center is efficiently polarized in the state $|0,+1/2\rangle$. This state crosses the state $|-1,-1/2\rangle$ precisely at 1024 G. These two states cannot be coupled directly by a transverse magnetic field because they have distinct nuclear-spin projections. However, they are indirectly coupled to each other via transverse-field-enabled coupling to the other two hyperfine-mixed states, which are superpositions of $|0,-1/2\rangle$ and $|-1,+1/2\rangle$. This situation is illustrated in Fig. 5(d), which shows the computed energy levels as a function of B_z in the presence of a finite transverse field (here, $B_\perp = 0.3$ G). The transverse field opens a gap between $|0,+1/2\rangle$ and $|-1,-1/2\rangle$ at 1024 G. As a consequence, they become mixed states which can give rise to coherent spin oscillations since optical pumping initializes the N-V center in the $|0,+1/2\rangle$ state. This situation is reminiscent of the ^{14}N-V case, where the 1024-G feature is due to an avoided crossing between two states coupled via a transverse magnetic field. The main difference here is that the coupling is indirect, mediated by two intermediate states. In the presence of magnetic noise, the coherent oscillations between the two coupled states are expected to be averaged out and appear as a decrease of the initial spin population, as we observe experimentally in this sample [Fig. 5(c)]. We note that a transverse-field-induced coupling also occurs at $B_z \approx 1027$ G, between $|0,+1/2\rangle$ and $|+\rangle \approx |0,-1/2\rangle$ [whose crossing is visible in Fig. 1(d), where no transverse field is included]. This coupling explains why the dynamic nuclear-spin polarization becomes ineffective around this field, as discussed in Sec. III (see Fig. 2).

An unfortunate consequence of the 1024-G feature of the ^{15}N-V center is that resonant coupling with a ^{1}H spin would normally occur very close to 1024 G since the Larmor frequency of ^{1}H is approximately 4.36 MHz at this field. Therefore, any signature of ^{15}N-$V-{}^1$H coupling would be overwhelmed by this strong intrinsic feature. It should be noted, however, that cross-relaxation resonances with nuclear spins should occur on both sides of the GSLAC [36] [see Fig. 1(b)], so that ^{1}H can still be detected before the GSLAC, at a magnetic field $B_z \approx 1022$ G. Moreover, improving the coherence properties (i.e., reducing the noise) of shallow N-V centers should significantly reduce the width and the amplitude of the 1024-G feature.

V. ALL-OPTICAL MAGNETIC-NOISE SPECTROSCOPY

By scanning the magnetic field across the GSLAC, we show that the transition frequency of the ^{14}N center can be tuned down to frequencies as low as 100 kHz in diamond samples with low intrinsic magnetic noise. This value is approximately an order of magnitude below the transition frequencies exhibited by nuclear species (e.g., ^{13}C) at 1024 G, thus creating the possibility for performing all-optical NMR spectroscopy by detecting cross-relaxation events between a probe N-V spin and target nuclear spins [36]. When the N-V transition frequency is matched to the nuclear Larmor frequency, the fluctuating nuclear field will cause the N-V spin to relax faster, translating into a decreased longitudinal relaxation time, T_1.

In order to test the possibility of detecting fluctuating magnetic fields near the GSLAC, we generate a local magnetic field by running an oscillating current through a wire placed in proximity to the diamond. To mimic nuclear-spin detection, we apply signals at various frequencies: 8 MHz, 4 MHz (approximate for ^{1}H or ^{19}F), 1 MHz (approximate for ^{13}C), and 500 kHz (approximate for ^{2}H or ^{17}O). The alternating current is modulated in amplitude and phase to ensure that the N-V center is not coherently driven but experiences noise from a randomly fluctuating current around a given frequency, similar to the signal from a possible target nuclear spin. The amplitude of the current is adjusted to obtain a root-mean-square field strength of

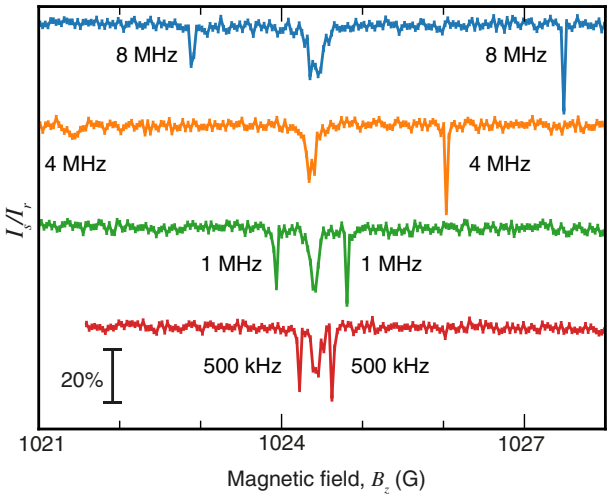

FIG. 6. PL scans across the GSLAC recorded with an evolution time $t = 10$ μs on the same ^{14}N-V center as in Fig. 3. For each scan, a magnetic noise is generated at central frequencies of 8 MHz, 4 MHz, 1 MHz, and 500 kHz, respectively (from the top down). The root-mean-square amplitude of the applied field is 1 μT. The curves are offset from each other for clarity.

1 μT, which corresponds approximately to the field generated by a dense organic sample of nuclear spins located at a 5-nm standoff distance [9]. The probe time is set to $t = 10$ μs to maximize the PL contrast. The resulting spectra (PL as a function of B_z), measured on a deep ^{14}N center in an isotopically purified CVD diamond, are shown in Fig. 6. While all frequencies are clearly detected after the GSLAC, the 4- and 8-MHz peaks are significantly weaker before the GSLAC. This effect is due to the N-V transitions being very weak in the (4–8)-MHz region because of the avoided crossing, as discussed previously (see Fig. 2). Past the GSLAC, however, there is no issue measuring any frequency, and thus NMR spectroscopy would be possible in this region for most commonly found nuclear-spin species. We note that the width of the resonances is governed here by the amplitude of the applied field (1 μT) through power broadening. Weaker signals produce narrower lines, down to the limit of spectral resolution imposed by spin dephasing, approximately $1/T_2^*$ [35], which is < 20 kHz in this sample. Reaching this limit is not possible in our experiment due to limited precision and stability of the applied magnetic field. This situation could be improved by using, e.g., an electromagnet [44].

VI. CONCLUSIONS

In this work, we investigate the photoinduced spin dynamics of N-V centers near the GSLAC. For the ^{14}N-V center, the spin transition frequency can be tuned down to values as low as 100 kHz in high-purity diamond. At the crossing (1024 G), we observe coherent spin oscillations caused by spin mixing induced by residual transverse magnetic fields. This spin mixing, in turn, limits the minimum accessible transition frequency exhibited by the environment. Measurements with shallow ^{14}N-V centers show that frequencies compatible with nuclear-spin signals (1–5 MHz) are within reach. For the ^{15}N-V center, the minimum transition frequency that is practically accessible is on the order of 2 MHz, governed by the avoided crossing intrinsic to the ^{15}N-V hyperfine structure. The ^{15}N-V center also exhibits a crossing feature at 1024 G, which is induced by transverse magnetic fields via an indirect hyperfine-mediated process. With this detailed understanding of the low-frequency spin dynamics around the GSLAC, we demonstrate all-optical spectroscopy of externally generated magnetic noise with frequencies ranging from 8 MHz down to 500 kHz, mimicking signals produced by precessing nuclear spins. This work thus paves the way towards all-optical, nanoscale NMR spectroscopy via cross-relaxation.

ACKNOWLEDGMENTS

We thank L. McGuinness for the experimental assistance with the diamond samples. This work was supported in part by the Australian Research Council (ARC) under the Centre of Excellence scheme (Project No. CE110001027). L. C. L. H. acknowledges the support of an ARC Laureate Fellowship (Project No. FL130100119). This work was performed in part at the Melbourne Centre for Nanofabrication (MCN) in the Victorian Node of the Australian National Fabrication Facility (ANFF).

[1] Aharon Blank, Curt R. Dunnam, Peter P. Borbat, and Jack H. Freed, High resolution electron spin resonance microscopy, J. Magn. Reson. **165**, 116 (2003).
[2] M. Poggio and C. L. Degen, Force-detected nuclear magnetic resonance: Recent advances and future challenges, Nanotechnology **21**, 342001 (2010).
[3] Yaron Artzi, Ygal Twig, and Aharon Blank, Induction-detection electron spin resonance with spin sensitivity of a few tens of spins, Appl. Phys. Lett. **106**, 084104 (2015).
[4] A. Bienfait, J. J. Pla, Y. Kubo, M. Stern, X. Zhou, C. C. Lo, C. D. Weis, T. Schenkel, M. L. W. Thewalt, D. Vion, D. Esteve, B. Julsgaard, K. Mølmer, J. J. L. Morton, and P. Bertet, Reaching the quantum limit of sensitivity in electron spin resonance, Nat. Nanotechnol. **11**, 253 (2015).
[5] L. Rondin, J.-P. Tetienne, T. Hingant, J.-F. Roch, P. Maletinsky, and V. Jacques, Magnetometry with nitrogen-vacancy defects in diamond, Rep. Prog. Phys. **77**, 056503 (2014).
[6] Romana Schirhagl, Kevin Chang, Michael Loretz, and Christian L. Degen, Nitrogen-vacancy centers in diamond: Nanoscale sensors for physics and biology, Annu. Rev. Phys. Chem. **65**, 83 (2014).
[7] Marcus W. Doherty, Neil B. Manson, Paul Delaney, Fedor Jelezko, Jörg Wrachtrup, and Lloyd C. L. Hollenberg, The nitrogen-vacancy colour centre in diamond, Phys. Rep. **528**, 1 (2013).
[8] L. P. McGuinness, Y. Yan, A. Stacey, D. A. Simpson, L. T. Hall, D. Maclaurin, S. Prawer, P. Mulvaney, J. Wrachtrup, F. Caruso, R. E. Scholten, and L. C. L. Hollenberg, Quantum measurement and orientation tracking of fluorescent nanodiamonds inside living cells, Nat. Nanotechnol. **6**, 358 (2011).
[9] T. Staudacher, F. Shi, S. Pezzagna, J. Meijer, J. Du, C. A. Meriles, F. Reinhard, and J. Wrachtrup, Nuclear magnetic resonance spectroscopy on a (5-nanometer)^3 sample volume, Science **339**, 561 (2013).
[10] Fazhan Shi, Xi Kong, Pengfei Wang, Fei Kong, Nan Zhao, Ren-Bao Liu, and Jiangfeng Du, Sensing and atomic-scale structure analysis of single nuclear-spin clusters in diamond, Nat. Phys. **10**, 21 (2013).
[11] C. Müller, X. Kong, J.-M. Cai, K. Melentijević, A. Stacey, M. Markham, D. Twitchen, J. Isoya, S. Pezzagna, J. Meijer, J. F. Du, M. B. Plenio, B. Naydenov, L. P. McGuinness, and F. Jelezko, Nuclear magnetic resonance spectroscopy with single spin sensitivity, Nat. Commun. **5**, 4703 (2014).
[12] S. Steinert, F. Ziem, L. T. Hall, A. Zappe, M. Schweikert, N. Götz, A. Aird, G. Balasubramanian, L. Hollenberg, and J. Wrachtrup, Magnetic spin imaging under ambient conditions with sub-cellular resolution, Nat. Commun. **4**, 1607 (2013).

[13] J.-P. Tetienne, T. Hingant, L. Rondin, A. Cavaillès, L. Mayer, G. Dantelle, T. Gacoin, J. Wrachtrup, J.-F. Roch, and V. Jacques, Spin relaxometry of single nitrogen-vacancy defects in diamond nanocrystals for magnetic noise sensing, Phys. Rev. B **87**, 235436 (2013).

[14] Stefan Kaufmann, David A. Simpson, Liam T. Hall, Viktor Perunicic, Philipp Senn, Steffen Steinert, Liam P. McGuinness, Brett C. Johnson, Takeshi Ohshima, Frank Caruso, Jörg Wrachtrup, Robert E. Scholten, Paul Mulvaney, and Lloyd Hollenberg, Detection of atomic spin labels in a lipid bilayer using a single-spin nanodiamond probe, Proc. Natl. Acad. Sci. U.S.A. **110**, 10894 (2013).

[15] A. Ermakova, G. Pramanik, J.-M. Cai, G. Algara-Siller, U. Kaiser, T. Weil, Y.-K. Tzeng, H. C. Chang, L. P. McGuinness, M. B. Plenio, B. Naydenov, and F. Jelezko, Detection of a few metallo-protein molecules using color centers in nanodiamonds, Nano Lett. **13**, 3305 (2013).

[16] A. O. Sushkov, N. Chisholm, I. Lovchinsky, M. Kubo, P. K. Lo, S. D. Bennett, D. Hunger, A. Akimov, R. L. Walsworth, H. Park, and M. D. Lukin, All-optical sensing of a single-molecule electron spin, Nano Lett. **14**, 6443 (2014).

[17] J. R. Maze, P. L. Stanwix, J. S. Hodges, S. Hong, J. M. Taylor, P. Cappellaro, L. Jiang, M. V. Gurudev Dutt, E. Togan, A. S. Zibrov, A. Yacoby, R. L. Walsworth, and M. D. Lukin, Nanoscale magnetic sensing with an individual electronic spin in diamond, Nature (London) **455**, 644 (2008).

[18] G. De Lange, D. Ristè, V. V. Dobrovitski, and R. Hanson, Single-Spin Magnetometry with Multipulse Sensing Sequences, Phys. Rev. Lett. **106**, 080802 (2011).

[19] L. P. McGuinness, L. T. Hall, A. Stacey, D. A. Simpson, C. D. Hill, J. H. Cole, K. Ganesan, B. C. Gibson, S. Prawer, P. Mulvaney, F. Jelezko, J. Wrachtrup, R. E. Scholten, and L. C. L Hollenberg, Ambient nanoscale sensing with single spins using quantum decoherence, New J. Phys. **15**, 073042 (2013).

[20] Jared H. Cole and Lloyd C. L. Hollenberg, Scanning quantum decoherence microscopy, Nanotechnology **20**, 495401 (2009).

[21] L. T. Hall, J. H. Cole, C. D. Hill, and L. C. L. Hollenberg, Sensing of Fluctuating Nanoscale Magnetic Fields Using Nitrogen-Vacancy Centers in Diamond, Phys. Rev. Lett. **103**, 220802 (2009).

[22] Abdelghani Laraoui, Jonathan S. Hodges, and Carlos A. Meriles, Magnetometry of random ac magnetic fields using a single nitrogen-vacancy center, Appl. Phys. Lett. **97**, 143104 (2010).

[23] Bernhard Grotz, Johannes Beck, Philipp Neumann, Boris Naydenov, Rolf Reuter, Friedemann Reinhard, Fedor Jelezko, Jörg Wrachtrup, David Schweinfurth, Biprajit Sarkar, and Philip Hemmer, Sensing external spins with nitrogen-vacancy diamond, New J. Phys. **13**, 055004 (2011).

[24] Abdelghani Laraoui, Jonathan S. Hodges, and Carlos A. Meriles, Nitrogen-vacancy-assisted magnetometry of paramagnetic centers in an individual diamond nanocrystal, Nano Lett. **12**, 3477 (2012).

[25] H. J. Mamin, M. H. Sherwood, and D. Rugar, Detecting external electron spins using nitrogen-vacancy centers, Phys. Rev. B **86**, 195422 (2012).

[26] Helena S. Knowles, Dhiren M. Kara, and Mete Atatüre, Observing bulk diamond spin coherence in high-purity nanodiamonds, Nat. Mater. **13**, 21 (2013).

[27] H. J. Mamin, M. Kim, M. H. Sherwood, C. T. Rettner, K. Ohno, D. D. Awschalom, and D. Rugar, Nanoscale nuclear magnetic resonance with a nitrogen-vacancy spin sensor, Science **339**, 557 (2013).

[28] M. Loretz, S. Pezzagna, J. Meijer, and C. L. Degen, Nanoscale nuclear magnetic resonance with a 1.9-nm-deep nitrogen-vacancy sensor, Appl. Phys. Lett. **104**, 033102 (2014).

[29] Stephen J. DeVience, Linh M. Pham, Igor Lovchinsky, Alexander O. Sushkov, Nir Bar-Gill, Chinmay Belthangady, Francesco Casola, Madeleine Corbett, Huiliang Zhang, Mikhail Lukin, Hongkun Park, Amir Yacoby, and Ronald L. Walsworth, Nanoscale NMR spectroscopy and imaging of multiple nuclear species, Nat. Nanotechnol. **10**, 129 (2015).

[30] K. Holliday, N. B. Manson, M. Glasbeek, and E. Van Oort, Optical hole-bleaching by level anti-crossing and cross relaxation in the N-V centre in diamond, J. Phys. Condens. Matter **1**, 7093 (1989).

[31] Seiji Armstrong, Lachlan J. Rogers, Roger L. McMurtrie, and Neil B. Manson, NV-NV electron-electron spin and NV-N_S electron-electron and electron-nuclear spin interaction in diamond, Phys. Procedia **3**, 1569 (2010).

[32] A. Jarmola, V. M. Acosta, K. Jensen, S. Chemerisov, and D. Budker, Temperature- and Magnetic-Field-Dependent Longitudinal Spin Relaxation in Nitrogen-Vacancy Ensembles in Diamond, Phys. Rev. Lett. **108**, 197601 (2012).

[33] Hai-Jing Wang, Chang S. Shin, Scott J. Seltzer, Claudia E. Avalos, Alexander Pines, and Vikram S. Bajaj, Optically detected cross-relaxation spectroscopy of electron spins in diamond, Nat. Commun. **5**, 4135 (2014).

[34] Toeno van der Sar, Francesco Casola, Ronald Walsworth, and Amir Yacoby, Nanometre-scale probing of spin waves using single-electron spins, Nat. Commun. **6**, 7886 (2015).

[35] L. T. Hall, P. Kehayias, D. A. Simpson, A. Jarmola, A. Stacey, D. Budker, and L. C. L. Hollenberg, Detection of nanoscale electron spin resonance spectra demonstrated using nitrogen-vacancy centre probes in diamond, Nat. Commun. **7**, 10211 (2016).

[36] James D. A. Wood, David A. Broadway, Liam T. Hall, Alastair Stacey, David A. Simpson, Jean-Philippe Tetienne, and Lloyd C. L. Hollenberg, Wide-band nanoscale magnetic resonance spectroscopy using quantum relaxation of a single spin in diamond, Phys. Rev. B **94**, 155402 (2016).

[37] Xing-Fei He, Neil B. Manson, and Peter T. H. Fisk, Paramagnetic resonance of photoexcited N-V defects in diamond. I. Level anticrossing in the ^3A ground state, Phys. Rev. B **47**, 8809 (1993).

[38] R. J. Epstein, F. M. Mendoza, Y. K. Kato, and D. D. Awschalom, Anisotropic interactions of a single spin and dark-spin spectroscopy in diamond, Nat. Phys. **1**, 94 (2005).

[39] Changjiang Wei and Neil B. Manson, Observation of the dynamic stark effect on electromagnetically induced transparency, Phys. Rev. A **60**, 2540 (1999).

[40] E. A. Wilson, N. B. Manson, and C. Wei, Perturbing an electromagnetic induced transparency within an inhomogeneously broadened transition, Phys. Rev. A **67**, 023812 (2003).

[41] G. D. Fuchs, G. Burkard, P. V. Klimov, and D. D. Awschalom, A quantum memory intrinsic to single nitrogen-vacancy centres in diamond, Nat. Phys. **7**, 789 (2011).

[42] Hai-Jing Wang, Chang S. Shin, Claudia E. Avalos, Scott J. Seltzer, Dmitry Budker, Alexander Pines, and Vikram S. Bajaj, Sensitive magnetic control of ensemble nuclear spin hyperpolarization in diamond, Nat. Commun. **4**, 1940 (2013).

[43] Ping Wang, Bao Liu, and Wen Yang, Strongly polarizing weakly coupled 13C nuclear spins with optically pumped nitrogen-vacancy center, Sci. Rep. **5**, 15847 (2015).

[44] Arne Wickenbrock, Huijie Zheng, Lykourgos Bougas, Nathan Leefer, Samer Afach, Andrey Jarmola, Victor M. Acosta, and Dmitry Budker, Microwave-free magnetometry with nitrogen-vacancy centers in diamond, Appl. Phys. Lett. **109**, 053505 (2016).

[45] S. Felton, A. M. Edmonds, M. E. Newton, P. M. Martineau, D. Fisher, D. J. Twitchen, and J. M. Baker, Hyperfine interaction in the ground state of the negatively charged nitrogen vacancy center in diamond, Phys. Rev. B **79**, 075203 (2009).

[46] H. Wieder and T. G. Eck, "Anticrossing" signals in resonance fluorescence, Phys. Rev. **153**, 103 (1967).

[47] A. Gruber, A. Dräbenstedt, C. Tietz, L. Fleury, J. Wrachtrup, and C. von Borczyskowski, Scanning confocal optical microscopy and magnetic resonance on single defect centers, Science **276**, 2012 (1997).

[48] N. B. Manson, J. P. Harrison, and M. J. Sellars, Nitrogen-vacancy center in diamond: Model of the electronic structure and associated dynamics, Phys. Rev. B **74**, 104303 (2006).

[49] J.-P. Tetienne, L. Rondin, P. Spinicelli, M. Chipaux, T. Debuisschert, J.-F. Roch, and V. Jacques, Magnetic-field-dependent photodynamics of single NV defects in diamond: An application to qualitative all-optical magnetic imaging, New J. Phys. **14**, 103033 (2012).

[50] V. Jacques, P. Neumann, J. Beck, M. Markham, D. Twitchen, J. Meijer, F. Kaiser, G. Balasubramanian, F. Jelezko, and J. Wrachtrup, Dynamic Polarization of Single Nuclear Spins by Optical Pumping of Nitrogen-Vacancy Color Centers in Diamond at Room Temperature, Phys. Rev. Lett. **102**, 057403 (2009).

[51] Viktor Ivády, Krisztián Szász, Abram L. Falk, Paul V. Klimov, David J. Christle, Erik Janzén, Igor A. Abrikosov, David D. Awschalom, and Adam Gali, Theoretical model of dynamic spin polarization of nuclei coupled to paramagnetic point defects in diamond and silicon carbide, Phys. Rev. B **92**, 115206 (2015).

[52] J. P. Colpa and D. Stehlik, Optical nuclear polarization as a consequence of the non-crossing rule (level-anti-crossing). I. Analytical treatment of ONP in the level-crossing region, Chem. Phys. **21**, 273 (1977).

[53] Gopalakrishnan Balasubramanian, Philipp Neumann, Daniel Twitchen, Matthew Markham, Roman Kolesov, Norikazu Mizuochi, Junichi Isoya, Jocelyn Achard, Johannes Beck, Julia Tissler, Vincent Jacques, Philip R. Hemmer, Fedor Jelezko, and Jörg Wrachtrup, Ultralong spin coherence time in isotopically engineered diamond, Nat. Mater. **8**, 383 (2009).

[54] L. T. Hall, J. H. Cole, and L. C. L. Hollenberg, Analytic solutions to the central-spin problem for nitrogen-vacancy centers in diamond, Phys. Rev. B **90**, 075201 (2014).

[55] J. R. Maze, A. Dréau, V. Waselowski, H. Duarte, J.-F. Roch, and V. Jacques, Free induction decay of single spins in diamond, New J. Phys. **14**, 103041 (2012).

[56] Ossi Lehtinen, Boris Naydenov, Pia Börner, Kristina Melentjevic, Christoph Müller, Liam Paul McGuinness, Sebastien Pezzagna, Jan Meijer, Ute Kaiser, and Fedor Jelezko, Molecular dynamics simulations of shallow nitrogen and silicon implantation into diamond, Phys. Rev. B **93**, 035202 (2016).

[57] R. Hanson, V. V. Dobrovitski, A. E. Feiguin, O. Gywat, and D. D. Awschalom, Coherent dynamics of a single spin interacting with an adjustable spin bath, Science **320**, 352 (2008).